Continuation Along Bifurcation Branches for a Tumor Model with a Necrotic Core

Wenrui Hao · Jonathan D. Hauenstein · Bei Hu · Yuan Liu · Andrew J. Sommese · Yong-Tao Zhang

Abstract We consider a free boundary problem for a system of partial differential equations, which arises in a model of tumor growth with a necrotic core. For any positive number R and $0 < \rho < R$, there exists a radially-symmetric stationary solution with tumor free boundary $r = R$ and necrotic free boundary $r = \rho$. The system depends on a positive parameter μ, which describes tumor aggressiveness, and for a sequence of values $\mu_2 < \mu_3 < \ldots$, there exist branches of symmetry-breaking stationary solutions, which bifurcate from these values. Upon discretizing this model, we obtain a family of polynomial systems parameterized by tumor aggressiveness factor μ. By continuously changing μ using a homotopy, we are able to compute nonradial symmetric solutions. We additionally discuss linear and nonlinear stability of such solutions.

W. Hao (✉) · B. Hu · Y. Liu · A.J. Sommese · Y.-T. Zhang
Department of Applied and Computational Mathematics and Statistics, University of Notre Dame,
Notre Dame, IN 46556, USA
e-mail: whao@nd.edu
url: www.nd.edu/~whao

B. Hu
e-mail: b1hu@nd.edu
url: www.nd.edu/~b1hu

Y. Liu
e-mail: yliu7@nd.edu
url: www.nd.edu/~yliu7

A.J. Sommese
e-mail: sommese@nd.edu
url: www.nd.edu/~sommese

Y.-T. Zhang
e-mail: yzhang10@nd.edu
url: www.nd.edu/~yzhang10

J.D. Hauenstein
Department of Mathematics, Texas A&M University, College Station, TX 77843-3368, USA
e-mail: jhauenst@math.tamu.edu
url: www.math.tamu.edu/~jhauenst

Springer

1 Introduction

Tumor growth models are challenging both from a theoretical and a numerical standpoint. The tumor and its boundary change over time in a way that is unknown in advance; one refers to the tumor boundary as a "free boundary." Mathematical models of tumor growth, which consider the tumor tissue as a density of proliferating cells, have been developed and studied. Basic continuous models are based on diffusion of nutrient, proliferation from growth and shrinkage from necroses due to lack of nutrient. Early models were produced by Greenspan [42, 43], and McEwain and Morris [52] in the 1970's. Since then a variety of tumor models appeared in the literature, taking into account cell-to-cell adhesion, avascular growth, angiogeneses, the formation of necrotic core, the presence of an inhibitor, etc., see [2, 9–12, 14, 15, 17, 20, 48, 51] and the references therein. Some nice review articles on this subject are [1, 13, 16, 18, 29, 30, 50]. In [7, 8, 10–12, 26–28, 31, 32, 39, 40, 42, 43], the free boundary is explicitly included as one of the unknowns (probably the most important unknown).

The focus for free boundary tumor models has been on the mathematical analysis. More specifically, there are a series of papers [7, 8, 27, 28, 31–40] that deal with bifurcation analysis and multiscale models for tumors with free boundary. A model with inhibitor was studied in [22], and models with necrotic core were considered in [10, 23].

A special case of the model, when $\mu = 0$, reduces to the Hele-Shaw problem with surface tension. The Hele-Shaw model cannot be used to model a tumor since, in reality, the tumor aggressiveness factor μ can never be 0. However, it is helpful for us to analyze the models using mathematical theories. For the Hele-Shaw problem the following results are well known: (i) for any smooth initial data there exists a unique solution with smooth boundary for a small time interval, while global existence is in general not expected; (ii) the only stationary solutions are spheres; (iii) spheres are asymptotically stable solutions, that is, for any smooth initial data "close" to that of a sphere, there exists a global smooth solution and solution that converges to a sphere as $t \rightarrow \infty$. The above three theoretical results for the Hele-Shaw model have been extended to the tumor model. Local existence and uniqueness was proved in [7, 8, 19]. In [39] it was shown that for any $0 < \widetilde{\sigma} < \underline{\sigma}$ there exists a unique radially-symmetric stationary solution, and its radius depends on $\widetilde{\sigma}/\underline{\sigma}$, but not on μ. Additionally, [40] shows for the 2-dimensional case that there exists a sequence of symmetric-breaking of stationary solutions bifurcating from μ_n ($n = 2, 3, 4, \ldots$). A general simplified proof, which works also for the 3-dimensional case, was given in [27]. The asymptotic stability of the spherical solution for $\mu < \mu_2$ and of the first bifurcation branch was studied extensively in [33, 34, 37]; earlier results for small μ were established in [8]. Stability of the problem was extensively studied in [33, 34, 37] for the radially-symmetric case as well as for nonradially-symmetric solutions in a small neighborhood of the first bifurcation branch. Stability results beyond this small neighborhood are nonexistent.

Bifurcation theory has been in applications of nonlinear PDEs. The existence of bifurcation points on given solution curves can be established by giving small perturbations of source solutions. If the perturbation is "small," the solution set of the perturbed problem should be somehow "close" to the solution set of the original problem. What happens near bifurcation points is much less obvious due to the singularity: will the bifurcations persist or will they "unfold"? This question depends on different problems. Although Crandall-Rabinowitz theorem can verify exactly the bifurcation points theoretically, it cannot be ap-

plied to complicated system such as the tumor model we study to explicitly compute the nonradially symmetric solution.

In the past several years, simulation of solid tumor models has increased dramatically. Nonlinear modeling has been performed to study the effects of shape instabilities on avascular [21], vascular and angiogenic [47, 55] solid tumor growth. The competition between heterogeneous cell proliferation and cell-to-cell and cell-to-matrix adhesion was studied in [20, 41]. In [49], a new adaptive boundary integral method to simulate the three dimensional solid tumor growth was developed. Additionally, [3] provides a computational method to deal with a high-dimension, multiscale models they developed. However, there is no efficient method to directly solve steady state systems for a free boundary problem and numerically study the bifurcation for the large scale system.

In this paper, we will consider a tumor model with necrotic core. Radial solutions of this model are given explicitly by analytical formulas in [44]. A radial shape models the tumors grown in vitro, but tumors in vivo may develop protrusions. It is therefore interesting to explore the existence of nonradial solutions of tumor models. Analytically finding nonradial solutions on a branch far from a radial solution is intractable. Another difficult question is to determine the stability of each solution, which will tell us whether the tumor is likely to spread. It is established in [44] that for a sequence of values $\mu_2 < \mu_3 < \ldots$, the radially-symmetric solutions bifurcate into nonradially-symmetric solutions. The values $\mu_2 < \mu_3 < \ldots$ are given explicitly by analytical formulas. The nonradial solutions near the bifurcation point are known up to the first order.

Even though this article studies a tumor growth model with a necrotic core, we propose a general numerical algorithmic approach to answer the following:

1. numerically compute values of the parameter where bifurcation occurs;
2. numerically compute nonspherical solutions on a branch far from the bifurcation; and
3. determine stability of these solutions.

The theoretical analysis of the bifurcation values $\mu = \mu_l$ provided in [44] allows us to check our numerical approach in this situation.

The contributions of this paper are:

- we introduce a numerical scheme to handle the tumor model with free boundaries;
- we develop a method to track the nonradial branch *beyond the small neighborhood* guaranteed by bifurcation theory and describe the solution behavior; and
- we implement a scheme for checking the stability of the nonradially-symmetric solutions we obtain.

The numerical algorithm we propose is based on recent developments in numerical algebraic geometry [5, 6, 54] and uses Bertini [4], a software package that implements numerical algebraic geometric algorithms. Roughly speaking, tumor models lead to systems of partial differential equations. We discretize these differential equations by incorporating the shape of the tumor utilizing a floating mesh with grid points on the moving boundary of the tumor. This leads to a system consisting of thousands of multivariate polynomials. To find bifurcation points of the spherical solutions as the tumor-aggressiveness factor μ changes, we track the spherical solution using μ as a continuous parameter monitoring the condition number of the Jacobian of the general system for not-necessarily-spherical solutions. Since the system must be degenerate at the bifurcation points, the condition number must be infinite at such points. Due to this rank deficiency, the computation requires using adaptive multiprecision path tracking [5, 6] (a feature currently only available with Bertini)

to perform computations in small neighborhoods of the bifurcation. Using a numerical approximation of the bifurcation point, we approximate the tangent cone to the family of solutions at the bifurcation point. Upon computing the tangent directions of the branch with nonradially-symmetric solutions, we use continuation to numerically track along the branch and compute the nonradially-symmetric solutions far along the branch. We also determine the stability of these solutions.

2 The Model

Mathematical models of solid tumor growth, which consider the tumor tissue as a density of proliferating cells, have been developed and studied in many papers, e.g., [1, 2, 8–10, 17, 23–25, 33, 39, 42, 43, 51, 52] and the references provided in them. Radially symmetric solutions have been extensively discussed, but non-spherical solutions of tumor models are also interesting.

If dead cells are not removed in an efficient manner from the tumor, they accumulate inside to form a necrotic core [17, 23]. A necrotic tumor growth model consists of a core of necrotic cells and a shell adjacent to this necrotic core of proliferating cells. In particular, let $\Omega(t)$ denote the tumor domain at time t, and $D(t) \subset \Omega(t)$ be the necrotic core within the tumor domain.

Let p be the pressure within the tumor resulting from proliferation of the tumor cells. The density of the cells, c, depends on the concentration of nutrients, σ, and, assuming that this dependence is linear, we simply identify c with σ. We also assume the proliferation rate, S, depends linearly upon σ in the living tumor region. That is,

$$S = \mu(\sigma - \widetilde{\sigma}) \quad \text{in } \Omega(t) \setminus D(t),$$

where $\widetilde{\sigma} > 0$ is a threshold concentration and μ is a positive parameter measuring the aggressiveness of the tumor. This equation represents the balance of the growth of the tumor by cell division and the contraction of the tumor by necrosis. First order Taylor expansion for the fully nonlinear model yields the linear approximation $\mu(\sigma - \widetilde{\sigma})$ used here.

We assume that there is no proliferation in the necrotic core, i.e, $S = 0$ in $D(t)$. Combining these two equations, we have

$$S = \mu(\sigma - \widetilde{\sigma})\chi_{\{\Omega(t)\setminus D(t)\}}(x) \quad \text{in } \Omega(t), \tag{2.1}$$

where $\chi_{\{\Omega(t)\setminus D(t)\}}(x)$ is the indicator function of the domain $\Omega(t) \setminus D(t)$, namely,

$$\chi_{\{\Omega(t)\setminus D(t)\}}(x) = \begin{cases} 1 & \text{if } x \in \Omega(t) \setminus D(t), \\ 0 & \text{otherwise.} \end{cases} \tag{2.2}$$

If we assume that necrotic cells do not consume nutrients and the consumption rate of nutrients by the living tumor cells is proportional to the concentration of the nutrients, then after normalization, σ satisfies

$$\sigma_t - \Delta\sigma = -\sigma \chi_{\{\Omega(t)\setminus D(t)\}}(x) \quad \text{in } \Omega(t) \quad \text{and} \quad \sigma = 1 \quad \text{on } \partial\Omega(t). \tag{2.3}$$

Additionally, if we assume that the density of cells in the necrotic core remains constant, and since we have assumed that the dependence between nutrient and density of the cell is linear, we have $\sigma = \underline{\sigma}$ in $D(t)$.

Most tumor models assume that the tissue has the structure of a porous medium so that Darcy's law holds. In particular, $\vec{v} = -\nabla p$ where $\vec{v}$ is the velocity of the cells and p is

the pressure. By conservation of mass, $\operatorname{div} \vec{v} = S = \mu(\sigma - \widetilde{\sigma})\chi_{\{\Omega(t)\setminus D(t)\}}(x)$ and thus $\Delta p = -\mu(\sigma - \widetilde{\sigma})\chi_{\{\Omega(t)\setminus D(t)\}}(x)$ in $\Omega(t)$. As in [15], the cell-to-cell adhesiveness condition at the tumor boundary is represented by $p = \kappa$ on $\partial\Omega(t)$, where κ is the mean curvature of the surface $\partial\Omega(t)$. See [53] for more details regarding the mean curvature. To simplify notation, we denote $\chi(x,t) = \chi_{\{\Omega(t)\setminus D(t)\}}(x)$. The necrotic core system is

$$
\begin{cases}
\sigma_t - \Delta\sigma = -\sigma\chi(x,t) \quad \text{and} \quad -\Delta p = \mu(\sigma - \widetilde{\sigma})\chi(x,t) & \text{in } \Omega(t), \\
\sigma = \underline{\sigma} & \text{on } \partial D(t), \\
\sigma = 1; \quad p = \kappa; \quad \text{and} \quad \frac{\partial p}{\partial n} = -V_n & \text{on } \partial\Omega(t),
\end{cases} \tag{2.4}
$$

where n denotes the exterior normal vector. Additionally, it is reasonable to assume $\underline{\sigma} < \widetilde{\sigma} < 1$. The steady-state system of the tumor model with a necrotic core is given as follows

$$
\Delta\sigma = \sigma\chi(x) \quad \text{in } \Omega, \tag{2.5}
$$

$$
-\Delta p = \mu(\sigma - \widetilde{\sigma})\chi(x) \quad \text{in } \Omega, \tag{2.6}
$$

$$
\sigma = \underline{\sigma} \quad \text{on } \partial D, \tag{2.7}
$$

$$
\sigma = 1 \quad \text{on } \partial\Omega, \tag{2.8}
$$

$$
p = \kappa \quad \text{on } \partial\Omega, \tag{2.9}
$$

$$
\frac{\partial p}{\partial n} = 0 \quad \text{on } \partial\Omega, \tag{2.10}
$$

where $\chi(x)$ is the indicator function of the domain $\Omega \setminus D$.

3 Discretization

It is known [44] that, for the original problem (2.5)–(2.10), bifurcation occurs at values $\mu = \mu_1, \mu_2, \ldots$. To demonstrate the applicability of numerical algebraic geometric methods to study free boundary problems, we will first describe how we generated a polynomial system by discretizing a 2-dimensional steady-state necrotic tumor model. Since this model has two free boundaries, we developed a novel approach to allow the grid to change in coordination with the two boundaries.

Let N_θ denote the number of fixed directions and $\theta_i = i \cdot \frac{2\pi}{N_\theta}$ for $i = 0, \ldots, N_\theta - 1$. Let r_i and ρ_i be the distance from the origin to the boundary of the tumor and the boundary of the necrotic core, respectively, in the θ_i direction. That is, r_i and ρ_i model the two free boundaries in the θ_i direction and can change independently.

We then discretize in each of these fixed directions both the necrotic region and the tumor region. Let N_ρ be the number of equally spaced grid points between the origin and each ρ_i and N_r be the number of equally spaced grid points between each ρ_i and r_i. Near the boundary of the tumor, we added two additional grid points that improve the accuracy of the discretization.

The location of all of the grid points change in accordance with the changing boundaries. For example, Fig. 1 presents the grid for a radial solution using $N_\theta = 40$, $N_\rho = 5$, and $N_r = 12$. Using the same setup, Fig. 2 presents a grid for a nonradial solution. The curve inside the region is the location of the necrotic core boundary.

We discretized the model described by (2.5)–(2.10) based on this moving grid using a third order finite difference scheme. The stencil of grid points consisted of the center point together with 14 surrounding points, which is presented in Fig. 3.

Fig. 1 Plot of a radially-symmetric grid with $N_\theta = 40$, $N_\rho = 5$, and $N_r = 12$
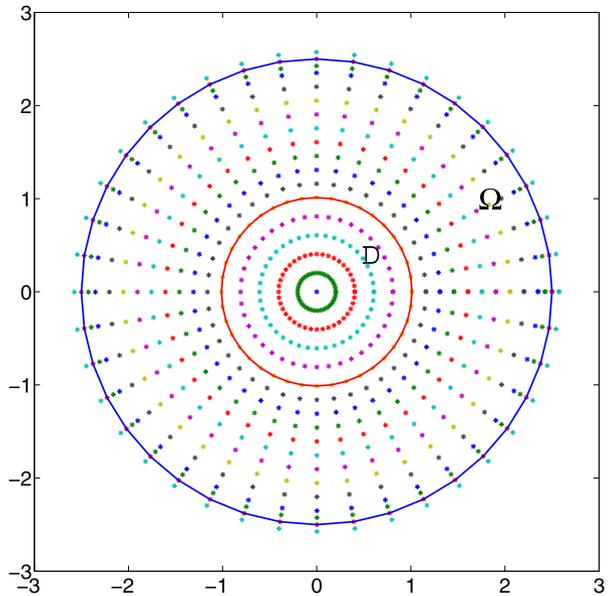
Fig. 2 Plot of a nonradially-symmetric grid with $N_\theta = 40$, $N_\rho = 5$, and $N_r = 12$
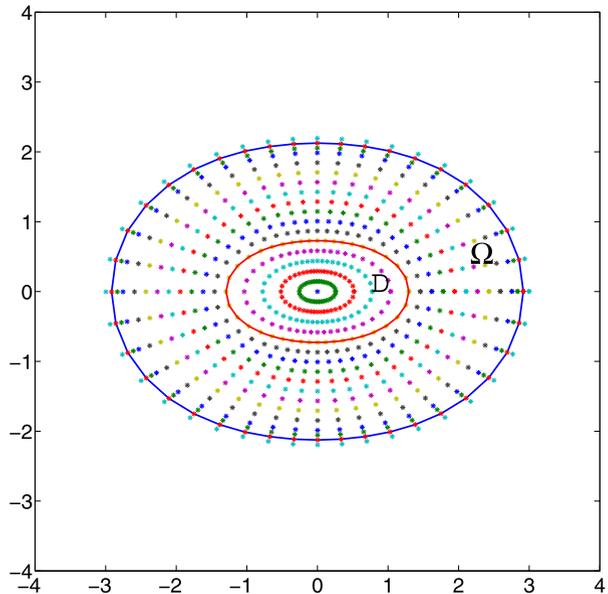
Using this stencil, we will now explicitly describe the discretization of σ with the discretization for p following similarly. To simplify, we will denote the location center grid point of the stencil as the origin. Let $d_{i,j}$ denote the distance from the jth grid point along the ith angular direction to the origin. The Taylor series expansion using the surrounding

grid points and values of σ yield a linear system

$$
\begin{bmatrix}
d_r(0,-2) & 0 \\
d_r(0,-1) & 0 \\
d_r(0,1) & 0 \\
d_r(0,2) & 0 \\
d_r(-2,0) & d_\theta(-2,0) \\
d_r(-1,0) & d_\theta(-1,0) \\
d_r(1,0) & d_\theta(1,0) \\
d_r(2,0) & d_\theta(2,0) \\
d_r(-2,-1) & d_\theta(-2,-1) \\
d_r(-1,-1) & d_\theta(-1,-1) \\
d_r(1,-1) & d_\theta(1,-1) \\
d_r(2,-1) & d_\theta(2,-1) \\
d_r(-1,-2) & d_\theta(-1,-2) \\
d_r(1,-2) & d_\theta(1,-2)
\end{bmatrix}
\begin{bmatrix}
\partial_r^{i,j}\sigma \\
\partial_{rr}^{i,j}\sigma \\
\partial_{rrr}^{i,j}\sigma \\
\partial_{rrrr}^{i,j}\sigma \\
\partial_\theta^{i,j}\sigma \\
\partial_{\theta\theta}^{i,j}\sigma \\
\partial_{r\theta}^{i,j}\sigma \\
\partial_{rr\theta}^{i,j}\sigma \\
\partial_{r\theta\theta}^{i,j}\sigma \\
\partial_{\theta\theta\theta}^{i,j}\sigma \\
\partial_{r\theta\theta\theta}^{i,j}\sigma \\
\partial_{rr\theta\theta}^{i,j}\sigma \\
\partial_{rrr\theta}^{i,j}\sigma \\
\partial_{\theta\theta\theta\theta}^{i,j}\sigma
\end{bmatrix}
=
\begin{bmatrix}
\sigma_{0,-2}-\sigma_{0,0} \\
\sigma_{0,-1}-\sigma_{0,0} \\
\sigma_{0,1}-\sigma_{0,0} \\
\sigma_{0,2}-\sigma_{0,0} \\
\sigma_{-2,0}-\sigma_{0,0} \\
\sigma_{-1,0}-\sigma_{0,0} \\
\sigma_{1,0}-\sigma_{0,0} \\
\sigma_{2,0}-\sigma_{0,0} \\
\sigma_{-2,-1}-\sigma_{0,0} \\
\sigma_{-1,-1}-\sigma_{0,0} \\
\sigma_{1,-1}-\sigma_{0,0} \\
\sigma_{2,-1}-\sigma_{0,0} \\
\sigma_{1,-2}-\sigma_{0,0} \\
\sigma_{-1,-2}-\sigma_{0,0}
\end{bmatrix},
$$

where

$$
d_r(i,j)=\left[d_{i,j},\frac{d_{i,j}^2}{2},\frac{d_{i,j}^3}{3!},\frac{d_{i,j}^4}{4!}\right]
$$

and

$$
d_\theta(i,j)=\left[i\Delta\theta,\frac{(i\Delta\theta)^2}{2},i\Delta\theta d_{i,j},\frac{d_{i,j}^2 i\Delta\theta}{2},\frac{d_{i,j}(i\Delta\theta)^2}{2},\frac{(i\Delta\theta)^3}{3!},\frac{d_{i,j}(i\Delta\theta)^3}{3!},\frac{d_{i,j}^2(i\Delta\theta)^2}{4},\right.
$$
$$
\left.\frac{d_{i,j}^3 i\Delta\theta}{3!},\frac{(i\Delta\theta)^4}{4!}\right].
$$

We obtain the derivatives by solving a linear system. Higher derivatives are only part of computation and are not used in discretization. Here we list the first and second derivatives with respect to r, which are denoted by $\partial_r^{i,j}$ and $\partial_{rr}^{i,j}$, respectively.

$\partial_r^{i,j}\sigma$

$$
=\frac{d_{i,j+1}d_{i,j+2}d_{i,j-1}d_{i,j-2}}{(d_{i,j-1}-d_{i,j-2})}\sum_{k=1}^{2}(-1)^k\frac{\sigma_{0,-k}}{d_{i,j-k}^2(d_{i,j+1}-d_{i,j-k})(d_{i,j+2}-d_{i,j-k})}
$$

$$
+\frac{d_{i,j-1}d_{i,j-2}d_{i,j+1}d_{i,j+2}}{(d_{i,j+1}-d_{i,j+2})}\sum_{k=1}^{2}(-1)^k\frac{\sigma_{0,k}}{d_{i,j+k}^2(d_{i,j+k}-d_{i,j-1})(d_{i,j+k}-d_{i,j-2})}
$$

$$
-\left(\frac{1}{d_{i,j+1}}+\frac{1}{d_{i,j+2}}+\frac{1}{d_{i,j-1}}-\frac{1}{d_{i,j-2}}\right)\sigma_{0,0},
$$

$\partial_{rr}^{i,j}\sigma$

$$
=2\left(\frac{d_{i,j+2}+d_{i,j-2}}{d_{i,j+2}d_{i,j-1}^2+d_{i,j-1}^2 d_{i,j-2}-d_{i,j-1}^3-d_{i,j-2}d_{i,j-1}d_{i,j+2}}\right.
$$

$$+ \frac{d_{i,j-1}d_{i,j+2} + d_{i,j-2}d_{i,j+2} + d_{i,j-1}d_{i,j-2}}{d_{i,j-1}(d_{i,j+1} - d_{i,j-1})(d_{i,j+2} - d_{i,j-1})(d_{i,j-1} - d_{i,j-2})} \Bigg) \sigma_{0,-1}$$

$$- 2 \frac{d_{i,j+2}d_{i,j+1} + d_{i,j-1}d_{i,j+1} + d_{i,j+2}d_{i,j-1}}{d_{i,j-2}(d_{i,j+1} - d_{i,j-2})(d_{i,j+2} - d_{i,j-2})(d_{i,j-1} - d_{i,j-2})} \sigma_{0,-2}$$

$$- 2 \frac{-d_{i,j+2}^3 d_{i,j-1}^2 + d_{i,j+2}^3 d_{i,j-2}^2 + d_{i,j+2}^2 d_{i,j-1}^3 - d_{i,j+2}^2 d_{i,j-2}^3 - d_{i,j-1}^3 d_{i,j-2}^2 + d_{i,j-2}^3 d_{i,j-1}^2}{d_{i,j+1}(d_{i,j+1} - d_{i,j+2})(d_{i,j+1} - d_{i,j-1})(d_{i,j+1} - d_{i,j-2})(d_{i,j+2} - d_{i,j-1})}$$

$$\times \frac{\sigma_{0,1}}{(d_{i,j+2} - d_{i,j-2})(d_{i,j-1} - d_{i,j-2})}$$

$$- 2 \frac{d_{i,j+1}d_{i,j-1} + d_{i,j-2}d_{i,j+1} + d_{i,j-2}d_{i,j-1}}{d_{i,j+2}(d_{i,j+1} - d_{i,j+2})(d_{i,j+2} - d_{i,j-1})(d_{i,j+2} - d_{i,j-2})} \sigma_{0,2}$$

$$\times 2 \left(\frac{d_{i,j+1} + d_{i,j+2} + d_{i,j-1}}{d_{i,j+1}d_{i,j+2}d_{i,j-1}} + \frac{d_{i,j+1}d_{i,j+2} + d_{i,j+1}d_{i,j-1} + d_{i,j+2}d_{i,j-1}}{d_{i,j+1}d_{i,j+2}d_{i,j-1}d_{i,j-2}} \right) \sigma_{0,0}.$$

We use a similar notation for partial derivatives with respect to θ. Since the discretization of these derivatives are straightforward but complicated, we have provided them at www.nd.edu/~sommese/preprints/scheme.m.

To avoid numerical difficulties with polar coordinates at the origin, we used Cartesian coordinates together with a central difference scheme at the origin. The variables of the resulting discretized system correspond to the location of the free boundaries in each direction along with the concentration of nutrients and pressure at each grid point. In particular, the number of variables of discretized system is $N_\theta(2(N_\rho + N_R) + 1) + 2$. To be more specific, define $\sigma_{i,j} = \sigma(\theta_i, r_j)$ and $p_{i,j} = p(\theta_i, r_j)$, for $i = 0, 1, 2, \ldots, N_\theta$ and $j = 0, 1, 2, \ldots, N_\rho + N_R$. The discretized system is

$$F(\sigma_{i,j}, p_{i,j}, r_i, \mu) = \begin{cases} \partial_{rr}^{i,j}\sigma + \frac{1}{r_{i,j}}\partial_r^{i,j}\sigma + \frac{1}{r_{i,j}^2}\partial_{\theta\theta}^{i,j}\sigma = \sigma_{i,j}\chi(j > N_\rho), \\ -(\partial_{rr}^{i,j}p + \frac{1}{r_{i,j}}\partial_r^{i,j}p + \frac{1}{r_{i,j}^2}\partial_{\theta\theta}^{i,j}p) = \mu(\sigma_{i,j} - \widetilde{\sigma})\chi(j > N_\rho), \\ \sigma_{i,N_\rho} = \underline{\sigma}, \\ \sigma_{i,N_R} = 1, \\ p = \kappa, \\ \partial_r^j p \partial_r^j \sigma + \partial_\theta^{i,j} p \partial_\theta^{i,j} \sigma \frac{1}{r_{i,j}^2} = 0, \\ \partial_r^{i,N_\rho} p^+ = \partial_r^{i,N_\rho} p^-, \end{cases} \tag{3.1}$$

where

$$\kappa|_{\partial\Omega} = \left(R(\partial_r^{i,N_R}\sigma)^2 (R\partial_r^{i,N_R}\sigma + \partial_{\theta\theta}^{i,N_R}\sigma) + (\partial_\theta^{i,N_R}\sigma)^2 (R\partial_{rr}^{i,N_R}\sigma + 2\partial_r^{i,N_R}\sigma) \right.$$

$$\left. - 2R\partial_r^{i,N_R}\sigma \partial_\theta^{i,N_R}\sigma \partial_{r\theta}^{i,N_R}\sigma \right) \Big/ \left(\sqrt{(R \, \partial_r^{i,N_R}\sigma)^2 + (\partial_\theta^{i,N_R}\sigma)^2} \right)^3.$$

In particular, all of the numerical derivatives are based on a third order finite difference scheme with $\partial_r^{i,N_\rho} p^+$ and $\partial_r^{i,N_\rho} p^-$ being the two sided derivatives. It should be emphasized that derivatives from each side of the dead-core boundary are computed using only grid points from one side and therefore the jump of second derivatives of σ and p does not impact this numerical computation. Since the derivatives involve r_j, these are described by rational functions. Clearing the denominators yields a polynomial system parameterized by μ.

Polar coordinates
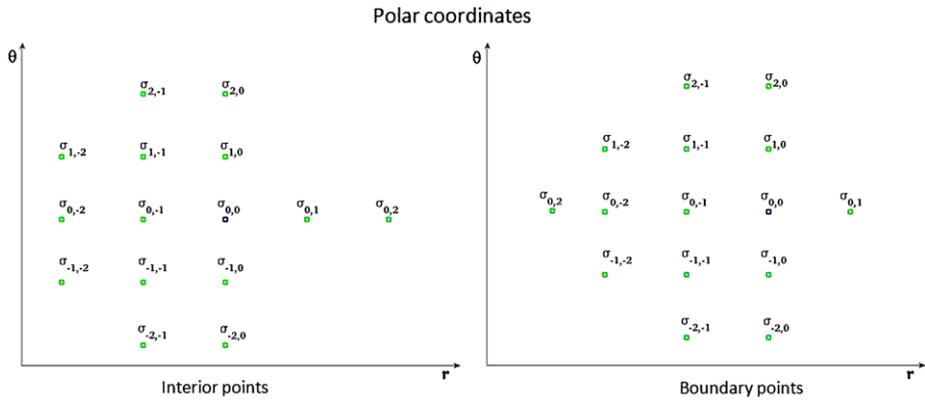
Fig. 3 Stencil for third order scheme

4 The Bifurcation Problem

Using the discretized problem described in Sect. 3, we want to numerically compute radially-symmetric and nonradially-symmetric solutions and, in particular, values of the parameter where bifurcations occur.

The first step is to compute radially-symmetric solutions for some fixed radius R and given parameter $\underline{\sigma}$. In this case, each $r_i = R$ and $\rho_i = P$ for some radius $0 < P < R$. In the radially-symmetric case, σ and p are independent of θ meaning that the discretized polynomial system simplifies extensively, namely,

$$\begin{cases} \partial_{rr}^j \sigma + \frac{1}{r_j}\partial_r^j \sigma = \begin{cases} \sigma_j, & j > N_\rho \\ 0, & j \le N_\rho \end{cases} \\ \partial_{rr}^j p + \frac{1}{r_j}\partial_r^j p = \begin{cases} -\mu(\sigma_j - \tilde{\sigma}), & j > N_\rho \\ 0, & j \le N_\rho \end{cases} \\ \sigma_{N_\rho} = \underline{\sigma}, \\ \sigma_{N_R} = 1, \\ p_{N_R} = \frac{1}{R}, \\ \partial_r^{N_R} p \partial_r^{N_R} \sigma = 0, \\ \partial_r^{N_\rho} p^+ = \partial_r^{N_\rho} p^-, \end{cases} \qquad (4.1)$$

where

$$\partial_r^j \sigma = \begin{cases} \dfrac{-\sigma_{0,2} + 8\sigma_{0,1} - 8\sigma_{0,-1} + \sigma_{0,-2}}{12\Delta R} & \text{interior points} \\[3mm] \dfrac{-\sigma_{0,2} + 20\sigma_{0,-1} + 16\sigma_{0,1} + 45\sigma_{0,0} - 80\sigma_{0,-2}}{30\Delta R} & \text{boundary point} \end{cases}$$

and

$$\partial_{rr}^j \sigma = \begin{cases} \dfrac{-\sigma_{0,2} + 16\sigma_{0,1} + 16\sigma_{0,-1} - \sigma_{0,-2} - 30\sigma_{0,0}}{12\Delta R^2} & \text{interior points} \\[3mm] \dfrac{-\sigma_{0,2} + 10\sigma_{0,-1} + 56\sigma_{0,1} - 105\sigma_{0,0} + 40\sigma_{0,-2}}{15\Delta R^2} & \text{boundary point.} \end{cases}$$

Table 1 Comparing (discretized) bifurcation value of μ_2 on a sequence of grids

Theoretical μ_2	N_θ	N_R	N_ρ	Numerical μ_2	Abs. error	Computing time
7.9772	40	10	5	7.9746	3e-3	30m29s
	48	12	6	7.9764	8e-4	41m54s
	64	16	8	7.9770	2e-4	70m23s

Table 2 Numerical error of radial symmetrical solution for $\mu = 8$ on a sequence of grids

N_θ	N_R	N_ρ	Numerical error
40	10	5	3.9876e-6
64	16	8	9.7339e-7
80	20	10	4.9838e-7

For a given value of N_ρ and μ, we solved this polynomial system using Bertini [4].

It is similar for the derivatives of function p. Upon computing the radially-symmetric solution for a given value of μ, the second step is to utilize the parameterization by μ of the polynomial system to determine the values where bifurcations occur. These values are located where the Jacobian of the discretized polynomial system is rank deficient. We utilized parameter continuation implemented in Bertini to look for such values by monitoring the condition number as μ varied. Figure 4 displays a graph of the condition number with respect to μ for $3 \leq \mu \leq 9$ where $R = 2.5$ and $\underline{\sigma} = 0.5$. In particular, we observe that the condition number spikes near $\mu = 7.98$ indicating the existence of a nearby singular radially-symmetric solution. Since higher precision arithmetic is often needed near a singularity to maintain the integrity of the floating point computations, we used the adaptive precision path tracking algorithms of [5, 6] implemented in Bertini to control the precision utilized for this computation. All the computations discussed here were run on a 2.33 GHz Intel Xeon 5410 processor running 64-bit Linux. Table 1 presents the time for the computation as well as the numerical error for computing μ_2 compared with the theoretical values provided explicitly in [44]. In Table 2, we consider three different grids and compare the error of the numerically computed radially-symmetric solution for $\mu = 8$ with the theoretical solution described in [44].

Given a numerical approximation of μ where the Jacobian is numerically rank deficient, the third step is to approximate the local tangent cone. This describes the tangent directions of the solution branches at the bifurcation. Due to the rank deficiency, this computation utilized multiprecision arithmetic. To simplify the notation, rewrite (3.1) as $F(x, \mu)$, where $x = (\sigma_{i,j}, p_{i,j}, r_i)$ for $i = 1, 2, \ldots, N_\theta$ and $j = 0, 1, \ldots, N_R + N_\rho$ are variables and μ is a parameter.

Given a polynomial system

$$f = \begin{bmatrix} f_1 \\ \vdots \\ f_m \end{bmatrix}$$

in $M + 1$ variables and a solution x^*, the tangent cone is the set of common zeroes of the lowest order terms of the Taylor expansions at x^* of the elements of the ideal generated by the polynomials $f_1, \ldots, f_m$. This is at first sight a difficult computation. In the special case when the Jacobian J_f of f evaluated at x^* has rank $M - 1$, then we know that the tangent
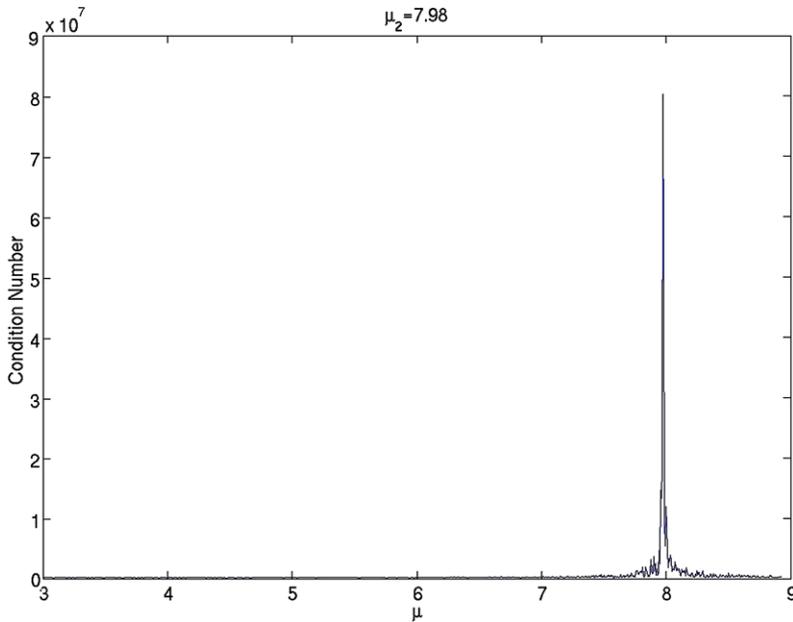
Fig. 4 Condition number with respect to μ for $R = 2.5$ and $\underline{\sigma} = 0.5$

cone lies in the two-dimensional linear space

$$\mathcal{V} := \left\{ v \in \mathbb{C}^{M+1} \mid J_f \cdot v = 0 \right\}.$$

If $\lambda \in \mathbb{C}^M$ is a nonzero row vector such that $\lambda \cdot J_f = 0$, it follows that all first order derivatives of $\lambda \cdot f$ vanish at x^*. We can compute the second order terms $\mathcal{Q}(x)$ of $\lambda \cdot f$ using the Hessian of $\lambda \cdot f$ at x^*. The tangent cone in question belongs to the solution set of $\mathcal{Q}$ on $\mathcal{V}$, and if this solution set is one-dimensional, it consists of either one or two lines. From this we conclude the tangent cone consists of at most two lines. In our case, using [44], we compute two lines, one in the direction of the radially-symmetric branch and the other in the direction of the nonradially-symmetric branch. We can use this direction with continuation to move onto the bifurcation branch.

The following algorithm computes these two tangent directions by reducing down to a polynomial in two variables utilizing an intrinsic parameterization of $\mathcal{V}$. The tangent directions then correspond to the two solutions of a polynomial system consisting of a homogeneous quadratic and a linear polynomial in two variables.

Procedure $(\Delta x_1, \Delta x_2) = \textbf{TangentCone}(F, \mu_0, x_0, \Delta_\mu)]$
Input A parameterized polynomial system $F(x, \mu)$, a parameter value μ_0, a point x_0 that is a singular solution of $F(x, \mu_0)$, and expected variation Δ_μ.
Output Two tangent directions Δx_1 and Δx_2.
Begin

  1. Compute the Jacobian matrix J_x with respect to the variables x and the derivative J_μ with respect to the parameter μ for F at (x_0, μ_0). Set $A := [J_x \ J_\mu]$.
  2. Compute a basis $\begin{bmatrix} q_1 & q_2 \\ u_1 & u_2 \end{bmatrix}$ for the two-dimensional null space of A and a nonzero vector λ in the one-dimensional null space of A^T.
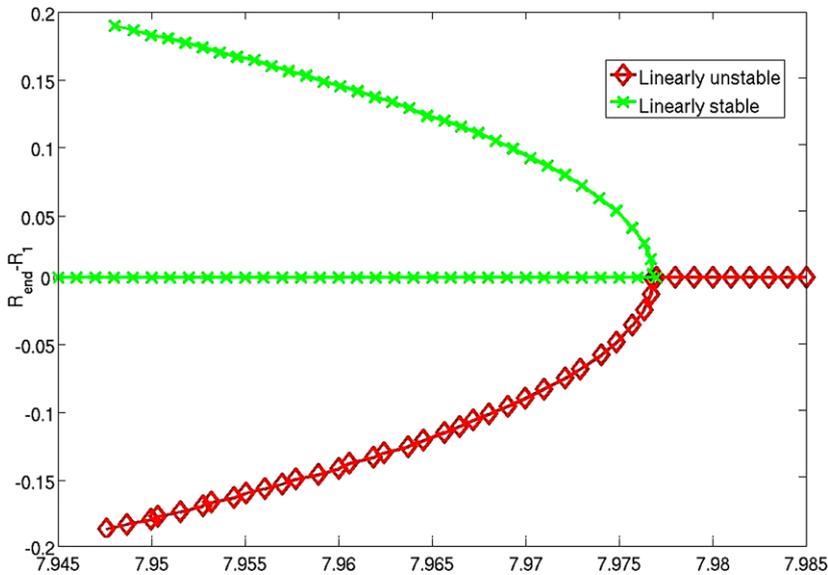
Fig. 5 Local behavior of the solution branches

3. Construct the polynomial $g(\alpha, \beta) = \lambda^T F(x_0 + \alpha q_1 + \beta q_2, \mu_0 + \alpha u_1 + \beta u_2)$.
4. Construct the Hessian matrix H of g and compute the two solutions (α_1, β_1) and (α_2, β_2) of the polynomial system

$$[\alpha, \beta] \cdot H(0, 0) \cdot [\alpha, \beta]^T = 0,$$

$$\alpha u_1 + \beta u_2 = \Delta_\mu.$$

Return $\Delta x_1 := \alpha_1 q_1 + \beta_1 q_2$ and $\Delta x_2 := \alpha_2 q_1 + \beta_2 q_2$.

After computing the tangent direction for the nonradially-symmetric solution branch, the last step is to track along that solution branch using the tangent direction as a first order description of the solution branch locally. After successfully moving off of the singularity and onto a smooth point on the solution branch, standard predictor-corrector methods were used to track along the solution branch. Figure 5 pictorially demonstrates the local behavior of the solution branches near the bifurcation at μ_2 for the running example. Figures 6 and 7 show the progression of the nonradial solution in each direction along the nonradially-symmetric solution branches. Even though the figures indicate that the "upper" and "lower" solution branches appear to differ only by a rotation, numerical values indicate that this is not the case and the next section shows that they indeed behave very differently.

5 Linear Stability Study

For the system (2.4), an important question is to determine the stability of the solution branches that we have computed. To that end, define $U^n = (\sigma_1(n\tau), p_1(n\tau), R_1(n\tau), \rho_1(n\tau))$ where τ is the time step size. We solved the linearized system of (2.4) described in [44] using a third order scheme in the spatial direction coupled with the backward Euler scheme in time direction. Such a scheme is unconditional stable. At each time step, this
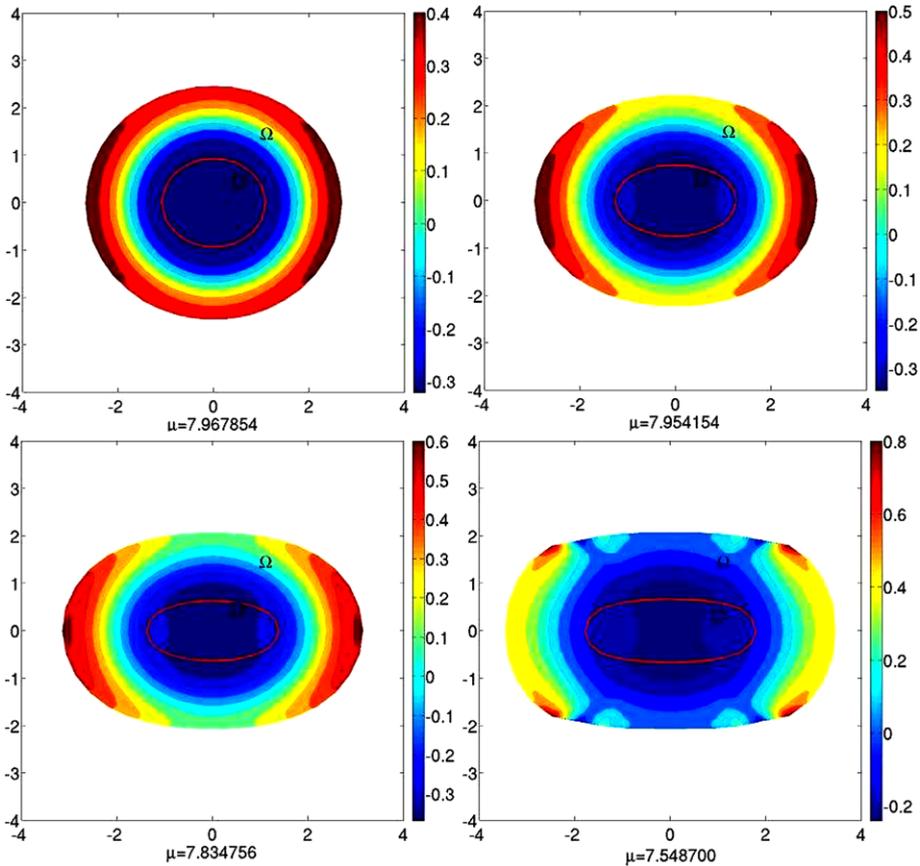
Fig. 6 Nonradially-symmetric "upper" branch

required the solving of the linear system $U^{n+1} = AU^n$, where the matrix A depends on the steady-state solutions (σ_0, p_0, R_0, ρ_0, see [44] for the detail) and τ. In particular, this process transfers the linear stability of the solution to the spectrum of the matrix A which depends upon the solution.

Let $|\rho(A)|$ denote the maximum absolute value of the eigenvalues of A. If $|\rho(A)| < 1$, then $\|U^n\| \to 0$ yielding a stable system. Additionally, if $|\rho(A)| > 1$, then the system is unstable. Since the stability of the radially-symmetric solutions has been determined [44], we are interested in the stability of the nonradially-symmetric solution branches.

For the working example, namely $R = 2.5$ and $\underline{\sigma} = 0.5$, we computed the eigenvalues of A for different values of μ along the "upper" and "lower" nonradially-symmetric solution branches to determine the stability. Tables 3 and 4 list $|\rho(A)|$ along the "upper" and "lower" branches, respectively. In particular, when $7.86654 < \mu < \mu_2 \approx 7.97689$, the "upper" branch is stable and, for μ near μ_2, the "lower" branch is unstable, as pictorially presented in Fig. 5. This computation shows that the top two solutions in Fig. 6 are stable while all the other solutions in Figs. 6 and 7 are unstable.

Since $|\rho(A)|$ is close to 1 for some of these computations, we verified the accuracy of the computations by doubling the number of grid points three times. The results of this
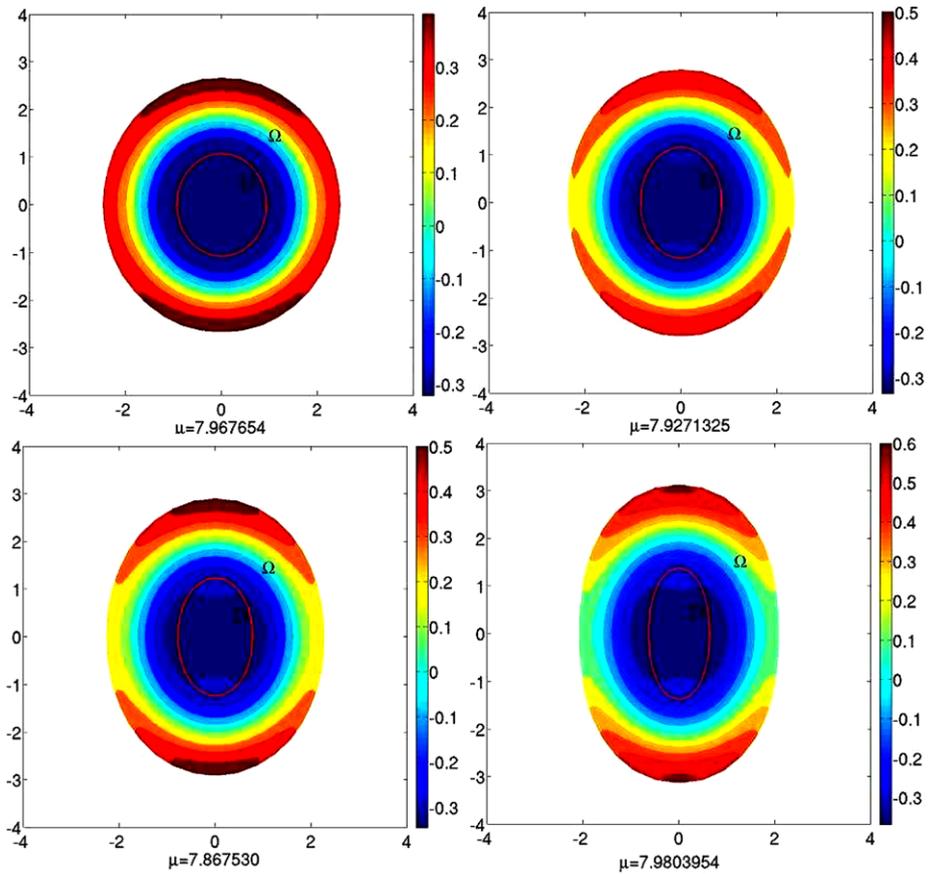
Fig. 7 Nonradially-symmetric "lower" branch

computation are presented in Table 5. In particular, the results described in this table together with Table 2 suggest that our numerical approximations have error on the order of 10^{-6} yielding that the linear stability is convincing and reasonable. Moreover, eigenvalue analysis is matched by time marching in our numerical simulation.

6 Nonlinear Stability Verification

By time marching the system (2.4), we numerically verified the nonlinear stability of the nonradially-symmetric solutions. This was accomplished by using a random perturbation of a nonradially-symmetric solution as the initial conditions for computing the steady-state solution. We used perturbations of the nonradially-symmetric solution of less than unit length and we just take two nonradially-symmetric solutions for explanation. Figure 8 demonstrates that the solution of $\mu = 7.882432$ ($|\rho(A)| = 0.99998$) converges back to the unperturbed solution, and that the solution of $\mu = 7.976203$ ($|\rho(A)| = 1.00002$) does not converge back to the unperturbed solution. Hence, we numerically verified that the nonlinear stability is consistent with the linear stability.
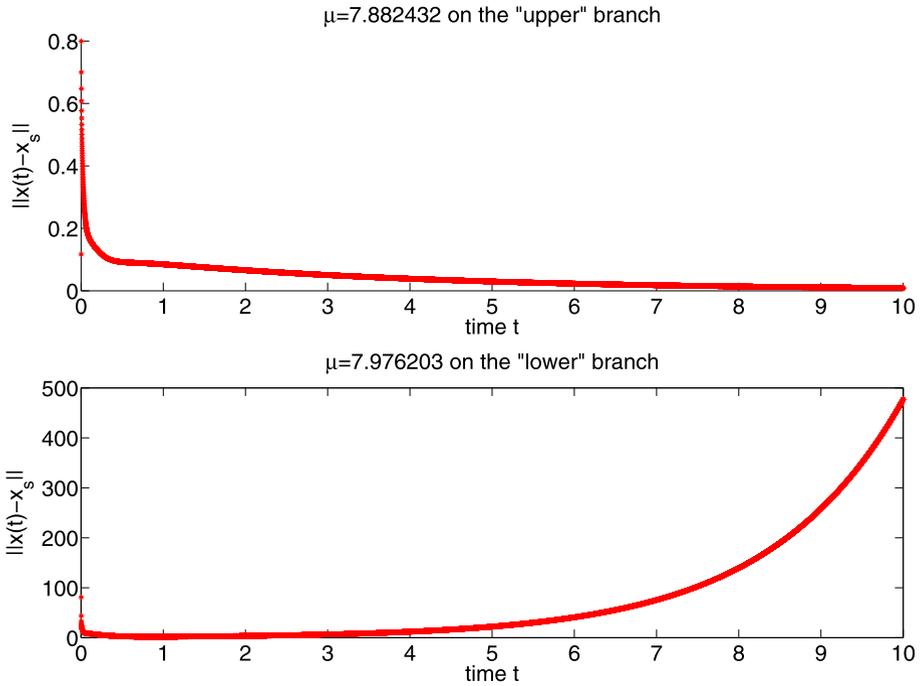
Fig. 8 Nonlinear stability

Table 3 Maximum eigenvalue for the "upper" branch

μ	$|\rho(A)|$	μ	$|\rho(A)|$	μ	$|\rho(A)|$
7.976889	1.00000	7.926135	0.99994	7.707620	1.00823
7.975754	0.99999	7.918189	0.99994	7.691728	1.03423
7.973053	0.99996	7.910243	0.99995	7.675836	1.06282
7.970353	0.99995	7.898324	0.99996	7.659944	1.09445
7.967654	0.99994	7.882432	0.99998	7.644052	1.12956
7.964954	0.99994	7.866540	1.00001	7.628160	1.16867
7.962254	0.99993	7.850648	1.00003	7.612268	1.21240
7.959554	0.99993	7.834756	1.00006	7.596376	1.26151
7.956854	0.99993	7.818864	1.00010	7.580484	1.31690
7.954154	0.99993	7.802972	1.00013	7.564592	1.37974
7.951454	0.99993	7.787080	1.00017	7.548700	1.45148
7.948754	0.99993	7.771188	1.00022	7.532808	1.53399
7.946054	0.99993	7.755296	1.00027	7.516916	1.62972
7.934081	0.99993	7.739404	1.00032	7.501024	1.74191

7 Conclusion

In this paper, we developed a new, finite difference method with homotopy tracking to compute steady states of tumor growth with a necrotic core. The tumor model we considered is

Table 4 Maximum eigenvalue for the "lower" branch

μ	$|\rho(A)|$	μ	$|\rho(A)|$	μ	$|\rho(A)|$
7.976889	1.00000	7.927133	1.00022	7.708590	1.08048
7.976203	1.00002	7.919186	1.00024	7.692696	1.10909
7.973553	1.00004	7.911239	1.00027	7.676802	1.14047
7.970903	1.00006	7.899318	1.00030	7.660908	1.17498
7.968253	1.00007	7.883424	1.00035	7.645014	1.21299
7.965603	1.00009	7.867530	1.00041	7.629120	1.25499
7.962953	1.00010	7.851636	1.00046	7.613226	1.30154
7.960303	1.00011	7.835742	1.00051	7.597332	1.35331
7.957653	1.00012	7.819848	1.00057	7.581438	1.41114
7.955003	1.00013	7.803954	1.00063	7.565544	1.47604
7.952353	1.00014	7.788060	1.00069	7.549650	1.54927
7.949703	1.00015	7.772166	1.00075	7.533756	1.63242
7.947053	1.00015	7.756272	1.00869	7.517862	1.72754
7.943027	1.00017	7.740378	1.03051	7.501968	1.83724

Table 5 Errors and orders

Formula	Value
$\max|x_{10} - x_{20}|$	$7.9414e{-}6$
$\max|x_{10} - x_{40}|$	$7.4104e{-}6$
$\max|x_{20} - x_{40}|$	$6.0829e{-}7$
$\max|x_{10} - x_{80}|$	$7.3657e{-}6$
$\max|x_{20} - x_{80}|$	$6.5529e{-}7$
$\max|x_{40} - x_{80}|$	$4.4882e{-}8$
$\log_2\left(\frac{\|x_{10}-x_{80}\|_2}{\|x_{20}-x_{80}\|_2}\right)$	2.6507
$\log_2\left(\frac{\|x_{20}-x_{80}\|_2}{\|x_{40}-x_{80}\|_2}\right)$	2.7477

a free boundary model with bifurcation phenomenon. The difficulty level of this problem is due to the free boundary and the singularity at bifurcation point. By using multi-precision arithmetic with homotopy tracking in Bertini, one can compute the bifurcation point numerically. Then tangent cone is used to compute the non-radially symmetric solution. This method is a general numerical algorithmic approach that can be applied to other free boundary problems, e.g., a three-dimensional tumor system [45] and a tumor system with a Stokes equation [46] have also been studied by this method.

The model discussed in this article has incorporated important physical quantities such as internal tumor pressure and cell-to-cell adhesion. The bifurcation diagram, Fig. 5, which was drawn using homotopy tracking, shows the local behavior of the steady state solutions. In particular, the stability analysis reveals that the stability of the tumor depends on how aggressive the tumor is, as measured by the size of the tumor aggressiveness factor μ. For the radially-symmetric branch, the tumor is stable for small μ and unstable for large μ. For the nonradially-symmetric branches, the "upper" branch is stable while the "lower" branch is unstable. The instability allows the tumor to increase its surface area, thereby allowing the tumor to grow larger. Instability means that the tumor may change shape and, in particular,

may grow into the surrounding tissue thereby becoming invasive [10, 11, 23]. In particular, we interpret the stability results to mean that the tumor will remain benign when stable and invasive when unstable.

Although the tumor model analyzed here is quite simple, this work provides a possible way to study the behavior of the tumor as the parameter changes. Moreover, the numerical approach provides a general method to study tumor growth systems with free boundaries by enabling one to compute nonradially-symmetric solutions and study their stability, both linear and nonlinear, beyond a small neighborhood of the bifurcation point. In early results, bifurcation theory was used to analyze the bifurcation branch, but only in a small neighborhood of the bifurcation point. In reality, tumor in vivo is unlikely to be of spherical shape. Thus, our tracking along the nonradial bifurcation branch in this paper may provide significant application.

References

1. Adam, J.A.: General aspect of modeling tumor growth and immune response. In: Adam, J.A., Bellomo, N. (eds.) A Survey of Models for Tumor-Immune System Dynamics, pp. 14–87. Birkhäuser, Boston (1996)
2. Adam, J.A., Maggelakis, S.A.: Diffusion regulated growth characteristics of a spherical prevascular carcinoma. Bull. Math. Biol. **52**, 549–582 (1990)
3. Ayati, B.P., Webb, G.F., Anderson, A.R.A.: Computational methods and results for structured multiscale models of tumor invasion. Multiscale Model. Simul. **5**, 1–20 (2005)
4. Bates, D.J., Hauenstein, J.D., Sommese, A.J., Wampler, C.W.: Bertini: Software for numerical algebraic geometry. Available at www.nd.edu/~sommese/bertini
5. Bates, D.J., Hauenstein, J.D., Sommese, A.J., Wampler, C.W.: Adaptive multiprecision path tracking. SIAM J. Numer. Anal. **46**, 722–746 (2008)
6. Bates, D.J., Hauenstein, J.D., Sommese, A.J., Wampler, C.W.: Stepsize control for path tracking. Contemp. Math. **496**, 21–31 (2009)
7. Bazally, B., Friedman, A.: A free boundary problem for elliptic-parabolic system: application to a model of tumor growth. Commun. Partial Differ. Equ. **28**, 517–560 (2003)
8. Bazally, B., Friedman, A.: Global existence and asymptotic stability for an elliptic-parabolic free boundary problem: an application to a model of tumor growth. Indiana Univ. Math. J. **52**, 1265–1304 (2003)
9. Britton, N., Chaplain, M.A.J.: A qualitative analysis of some models of tissue growth. Math. Biosci. **113**, 77–89 (1993)
10. Byrne, H.M., Chaplain, M.A.J.: Growth of nonnecrotic tumors in the presence and absence of inhibitors. Math. Biosci. **130**, 151–181 (1995)
11. Byrne, H.M., Chaplain, M.A.J.: Growth of nonnecrotic tumors in the presence and absence of inhibitors. Math. Biosci. **135**, 187–216 (1996)
12. Byrne, H.M., Chaplain, M.A.J.: Free boundary value problems associated with growth and development of multicellular spheroids. Eur. J. Appl. Math. **8**, 639–658 (1997)
13. Bellomo, N., Preziosi, L.: Modelling and mathematical problems related to tumor evolution and its interaction with the immune system. Math. Comput. Model. **32**, 413–452 (2000)
14. Byrne, H.M.: The importance of intercellular adhesion in the development of carcinomas. IMA J. Math. Appl. Med. Biol. **14**, 305–323 (1997)
15. Byrne, H.M., Chaplain, M.A.J.: Modelling the role of cell-cell adhesion in the growth and development of carcinomas. Math. Comput. Model. **12**, 1–17 (1996)
16. Byrne, H.M.: Mathematical modelling of solid tumour growth: from avascular to vascular, via angiogenesis. Math. Biol. **14**, 219–287 (2009)
17. Chaplain, M.A.J.: The development of a spatial pattern in a model for cancer growth. In: Othmer, H.G., Maini, P.K., Murray, J.D. (eds.) Experimental and Theoretical Advances in Biological Pattern Formation, pp. 45–60. Plenum, New York (1993)

18. Chaplain, M.A.J.: Modelling aspects of cancer growth: insight from mathematical and numerical analysis and computational simulation. In: Multiscale Problems in the Life Sciences. Lecture Notes in Math., vol. 1940, pp. 147–200. Springer, Berlin (2008)
19. Chen, X., Friedman, A.: A free boundary problem for elliptic-hyperbolic system: an application to tumor growth. SIAM J. Math. Anal. **35**, 974–986 (2003)
20. Cristini, V., Frieboes, H.B., Gatenby, R., Caserta, S., Ferrari, M., Sinek, J.: Morphologic instability and cancer invasion. Clin. Cancer Res. **11**, 6772–6779 (2005)
21. Cristini, V., Lowengrub, J., Nie, Q.: Nonlinear simulation of tumor growth. J. Math. Biol. **46**, 191–224 (2003)
22. Cui, S., Friedman, A.: Analysis of a mathematical model of the effect of inhibitors on the growth of tumors. Math. Biosci. **164**, 103–137 (2000)
23. Cui, S., Friedman, A.: Analysis of a mathematical model of the growth of necrotic tumors. Aust. J. Math. Anal. Appl. **255**, 636–677 (2001)
24. Cui, S., Escher, J.: Bifurcation analysis of an elliptic free boundary problem modelling the growth of avascular tumors. SIAM J. Math. Anal. **39**, 210–235 (2007)
25. Cui, S., Escher, J.: Asymptotic behaviour of solutions of a multidimensional moving boundary problem modeling tumor growth. Commun. Partial Differ. Equ. **32**, 636–655 (2008)
26. Franks, S.J.H., King, J.R.: Interaction between a uniformly proliferating tumor and its surroundings: uniform material properties. Math. Med. Biol. **20**, 47–89 (2003)
27. Fontelos, M., Friedman, A.: Symmetry-breaking bifurcations of free boundary problems in three dimensions. Asymptot. Anal. **35**, 187–206 (2003)
28. Friedman, A.: A free boundary problem for a coupled system of elliptic, parabolic and stokes equations modeling tumor growth. Interfaces Free Bound. **8**, 247–261 (2006)
29. Friedman, A.: A hierarchy of cancer models and their mathematical challenges. Mathematical models in cancer. Discrete Contin. Dyn. Syst., Ser. B **4**, 147–159 (2004)
30. Friedman, A.: Mathematical analysis and challenges arising from models of tumor growth. Math. Models Methods Appl. Sci. **17**, 1751–1772 (2007)
31. Friedman, A.: A multiscale tumor model. Interfaces Free Bound. **10**, 245–262 (2008)
32. Friedman, A.: Free boundary problems associated with multiscale tumor models. Math. Model. Nat. Phenom. **4**, 134–155 (2009)
33. Friedman, A., Hu, B.: Bifurcation from stability to instability for a free boundary problem arising in a tumor model. Arch. Ration. Mech. Anal. **180**, 293–330 (2006)
34. Friedman, A., Hu, B.: Asymptotic stability for a free boundary problem arising in a tumor model. J. Differ. Equ. **227**, 598–639 (2006)
35. Friedman, A., Hu, B.: Bifurcation for a free boundary problem modeling tumor growth by stokes equation. SIAM J. Math. Anal. **39**, 174–194 (2007)
36. Friedman, A., Hu, B.: Bifurcation from stability to instability for a free boundary problem modeling tumor growth by stokes equation. J. Math. Anal. Appl. **327**, 643–664 (2007)
37. Friedman, A., Hu, B.: Stability and instability of Liapunov-Schmidt and Hopf bifurcation for a free boundary problem arising in a tumor model. Trans. Am. Math. Soc. **360**, 5291–5342 (2008)
38. Friedman, A., Kao, C.-Y., Hu, B.: Cell cycle control at the first restriction point and its effect on tissue growth. J. Math. Biol. **60**, 881–907 (2010)
39. Friedman, A., Reitich, F.: Analysis of a mathematical model for growth of tumor. J. Math. Biol. **38**, 262–284 (1999)
40. Friedman, A., Reitich, F.: Symmetry-breaking bifurcation of analytic solutions to free boundary problems: an application to a model of tumor growth. Trans. Am. Math. Soc. **353**, 1587–1634 (2000)
41. Frieboes, H.B., Zheng, X., Sun, C.-H., Tromberg, B., Gatenby, R., Cristini, V.: An integrated computational/experimental model of tumor invasion. Cancer Res. **66**, 1597–1604 (2006)
42. Greenspan, H.P.: Models for the growth of a solid tumor by diffusion. Stud. Appl. Math. **52**, 317–340 (1972)
43. Greenspan, H.P.: On the growth of cell culture and solid tumors. Theor. Biol. **56**, 229–242 (1976)
44. Hao, W., Hauenstein, J.D., Hu, B., Liu, Y., Sommese, A.J., Zhang, Y.-T.: Bifurcation of steady-state solutions for a tumor model with a necrotic core. Nonlinear Analysis Ser. B, Real World Appl. **13**, 694–709 (2012)
45. Hao, W., Hauenstein, J.D., Hu, B., Sommese, A.J.: A three-dimensional steady-state tumor system. Appl. Math. Comput. **218**, 2661–2669 (2011)
46. Hao, W., Hauenstein, J.D., McCoy, T., Hu, B., Sommese, A.J.: Computing steady-state solutions for a free boundary problem modeling tumor growth by stokes equation (submitted). Available at www.nd.edu/~sommese/preprints
47. Hogea, C.S., Murray, B.T., Sethian, J.A.: Simulating complex tumor dynamics from avascular to vascular growth using a general level-set method. J. Math. Biol. **53**, 86–134 (2006)

48. Lejeune, O., Chaplain, M.A.J., El Akili, I.: Oscillations and bistability in the dynamics of cytotoxic reactions mediated by the response of immune cells to solid tumours. Math. Comput. Model. **47**, 649–662 (2008)
49. Li, X., Cristini, V., Nie, Q., Lowengrub, J.: Nonlinear three-dimensional simulation of solid tumor growth. Discrete Contin. Dyn. Syst., Ser. B **7**, 581–604 (2007)
50. Lowengrub, J.S., Frieboes, H.B., Jin, F., Chuang, Y.-L., Li, X., Macklin, P., Wise, S.M., Cristini, V.: Nonlinear modelling of cancer: bridging the gap between cells and tumours. Nonlinearity **23**, 1–91 (2010)
51. Maggelakis, S.A., Adam, J.A.: Mathematical model for prevascular growth of a spherical carcinoma. Math. Comput. Model. **13**, 23–38 (1990)
52. McEwain, D.L.S., Morris, L.E.: Apoptosis as a volume loss mechanism in mathematical models of solid tumor growth. Math. Biosci. **39**, 147–157 (1978)
53. Weisstein, E.W.: Mean curvature. From MathWorld–A. Wolfram Web Resource. Available at mathworld.wolfram.com/MeanCurvature.html
54. Sommese, A.J., Wampler, C.W.: Numerical Solution of Systems of Polynomials Arising in Engineering and Science. World Scientific, Singapore (2005)
55. Zheng, X., Wise, S.M., Cristini, V.: Nonlinear simulation of tumor necrosis, neovascularization and tissue invasion via an adaptive finite-element/level-Set method. Bull. Math. Biol. **67**, 211–259 (2005)